

# Shreya Hegde Final Pioneer Paper.pdf

*by Shreya Hegde*

---

**Submission date:** 12-Aug-2021 04:41PM (UTC-0400)

**Submission ID:** 1630727988

**File name:** Shreya\_Hegde\_Final\_Pioneer\_Paper.pdf (6.95M)

**Word count:** 7813

**Character count:** 40431

# How sensitive is optimal matched filtering to spin parameters in a template?

Shreya Hegde

Pioneer Academics under Professor Eric Myer's supervision

(Dated: 12th August 2021)

## Abstract

The goal of this project would be to evaluate how the changes in waveform template parameters affect the detection efficiency of a black hole event. I recovered some of the main gravitational-wave event detections, ran the detection process using optimal matched filtering, changed the parameters, particularly the spin, and got slightly different waveform templates. I then drew conclusions about the nature of approximants and template banks I used through the signal-to-noise ratio results. Finally, I generated fake strains having the same parameters as the actual event signal to evaluate the effect of noise in our event's signal on change in SNR. The paper discusses how using different waveform models gives us very different templates and how having a high SNR value doesn't necessarily guarantee complete overlap between the template and signal. Generating a fake strain with the same parameters as the actual strain and varying the template's spin leads to slightly different SNR vs.  $\text{spin}1z$  vs.  $\text{spin}2z$  surface plots. Moreover, since there is a relationship between  $\text{spin}1z$  and  $\text{spin}2z$ , we see that the shape of the 3D plot between SNR,  $\text{spin}1z$ , and  $\text{spin}2z$  is the same as the shape of the 2D plot between SNR and  $\text{spin}1z+\text{spin}2z$ .

## INTRODUCTION

Understanding gravitational waves signals is crucial for us as they give us a lot of information about binary black hole systems and, in turn, even stellar evolution. It is challenging to study these systems via any other means. A black hole's properties are mass (how much it bends spacetime), electric charge (positive, negative, or neutral), and spin (how much it spins spacetime around). We can calculate the spin by evaluating the effect of the black hole's angular momentum that whirls spacetime on the surrounding space and objects. It gives us insights into how a black hole was born and how it grew.

My project deals with gaining a deeper insight into the relationship between the spin of the two black holes in a binary black hole system and the peak in the signal-to-noise time series for our template used in the gravitational-wave signal detection. I am dividing my analysis into four different sections: checking how the signal-to-noise ratio changes with the change in the spin values and the waveform model used, comparing the posterior samples from PyCBC with my results, examining how the plots change if I generate a fake signal (i.e., in the absence of noise) and do matched filtering with a template, and verifying my results by checking if there is a residue when I subtract the template from the data.

### Background

In 1916 gravitational waves were predicted by Albert Einstein in his general theory of relativity. Einstein claimed and showed that gravity is not force but instead the warping of spacetime. An accelerating object ends up distorting the curvature of spacetime around it, and these distortions travel away from this source at the speed of light in the form of waves. These waves are gravitational waves. This is very similar to how moving electrons produce electromagnetic waves and vibrating air particles produce sound waves. The gravitational field's changing strength is analogous to changing electric and magnetic fields (in electromagnetic waves) and varying air pressure (in sound waves).

Learning about gravitational waves is like listening to sound through our ears. This is entirely different from studying electromagnetic waves (similar to seeing with our eyes). Moreover, unlike electromagnetic waves, gravitational waves travel through the Universe unrestricted as they interact very weakly with matter. This provides us "pure" information

free from modifications. The waves provide us with invaluable information that could not have been possible with other ways of detection. Moreover, gravitational wave detections offer an independent way to calculate the tricky Hubble constant.

Thus, many have tried to detect gravitational waves through the past century. Joe Weber developed the first gravitational-wave detectors (Weber bars) by pioneering the use of resonant bars at room temperature in the 1960s. In 1974, astronomers Joe Taylor and Russell Hulse discovered the first binary pulsar using the 300-m radio telescope at Arecibo. The two stars' orbit was shrinking at the rate of 1 cm/day. Taylor and Hulse won the 1993 Nobel Prize for showing that the loss in orbital energy due to this shrinkage is converted to gravitational waves. This was useful in proving that Einstein was indeed right with his predictions in the general theory of relativity. [1]

## **LIGO**

Resonant detectors and previous methods of detection were not sensitive enough to detect gravitational waves. Gravitational-wave interferometric detectors outperformed resonant detectors in the 2000s as they promised better sensitivity. As gravitational waves cause a distortion in spacetime itself, people realized that they could send a laser beam to measure the space between two objects moving back and forth and find the time this pulse takes to come back. This is the principle on which LIGO, Laser Interferometer Gravitational-Wave Observatory, is based. It is the world's largest gravitational-wave observatory and consists of L-shaped laser interferometers 3000 km apart from one another.

Interferometers are devices that create an interference pattern. Interference is the wave produced by the addition of amplitudes at each point of each wave that is being superimposed. There are two types of interference: constructive and destructive interference. Total constructive interference occurs when the crests (maximum amplitude) and troughs (minimum amplitude) of the waves perfectly add up. Total destructive interference happens when every crest matches every trough of two waves that are alike. This leads to the waves canceling each other. When the waves are not perfectly matching, partial constructive or destructive interference is detected.

Since gravitational waves stretch and squeeze the fabric of spacetime (at a 90 degree angle to each other by 1 part in 10<sup>19</sup>, i.e., 10,000 times smaller than a proton), they change the

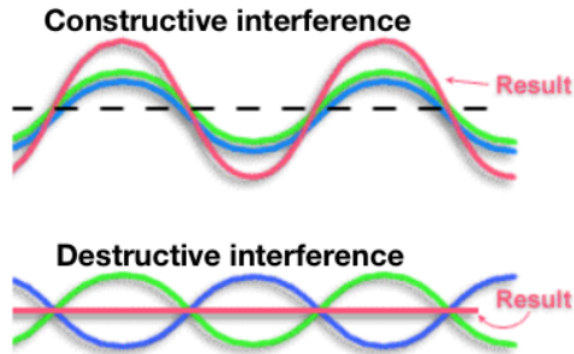


FIG. 1: Interference [2]

interferometer's arms' length when they pass through it. One arm gets longer while the other gets shorter. These tiny wiggles are very hard to detect until the arms of the interferometer are very long. Thus, LIGO arms are 4 kilometers long. Action at the interferometer begins with an input beam. A 45 degree tilted beam splitter (a partially reflective mirror) splits it into two separate beams. LIGO modified the simple Michelson's design interferometer to include "Fabry Perot cavities" to help solve the limitations caused by even the 4km long LIGO arms by increasing the distance traveled by lasers to 1200km (with increasing the reflections) and building the laser's intensity. A power recycling mirror helps increase the initial 40W laser to 750kW. Building a laser with a 750 km initial power is a practical impossibility. This increased laser power ensures that we see sharpened interference bands, in turn making it easier to detect.

Due to the continuous change in the length of interferometer arms when a gravitational-wave passes through it, the distance traveled by the laser changes. The laser beam in the shorter arm comes back before the laser in the other arm. The photodetector detects a flicker of light as the waves are not in alignment when they interfere with at beam splitter. This is how gravitational waves are detected.

### Detection

On September 14th, 2015, LIGO physically sensed the distortions caused by the gravitational waves in the fabric of spacetime. The collision between two black holes 1.3 billion

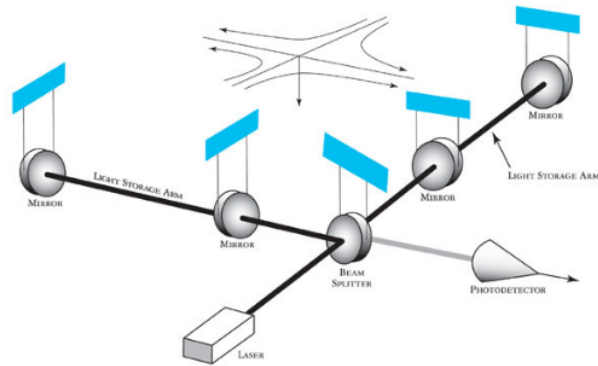


FIG. 2: Design of the LIGO interferometers [3]

light-years away lasted 20 milliseconds. The total power released in that short period was 50 times larger than the power of all the stars in the universe combined. The gravitational waves traveled 1.3 billion years to the Earth. The signal was recorded at both Livingston and Hanford, with a seven milliseconds difference (as they are 3000 km apart) in the event's recording. This was the first time humans have ever observed a binary black hole system.

Only three black hole mergers were detected in the first observing run (September 2015 to January 2016). In the second observing run (November 2016 to August 2017), eight events were observed: seven black hole mergers and one (the first) neutron star merger. In the third observing run (April 2019 to March 2020), a second neutron star merger and 38 BBH mergers were detected [9] bringing the total to 50 events. The next observing run (late 2021 or early 2022) will have upgrades to increase the sensitivity by about 60 percent for Hanford and 40 percent for Livingston [9].

### Background noise

The interferometer noise floor is caused by the fundamental noise sources, quantum noise, and thermal noise. Thermal noise is determined by permanent parameters, such as material properties and beam size. Since the mirrors are kept at room temperature, there's some thermal noise. Secondly, the beam is influenced by quantum fluctuations in space itself. Quantum noise depends on the readily variable input laser power and the changeable signal recycling mirror transmission. Laser frequency or amplitude noise, photodetector dark noise,

actuator noise, etc., are called technical noises. [4]

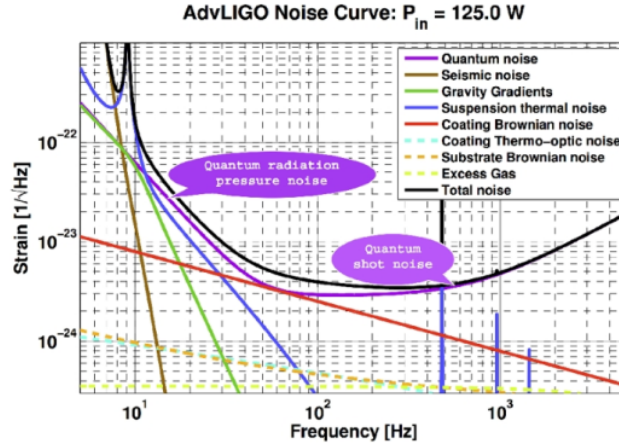


FIG. 3: Principal noise terms [5]

The 40-kg mirrors (test masses) at LIGO, made of fused silica, are the most reflective in the world as they absorb one in every 3.3 million photons to prevent heating and shape changes. After the 4W laser's origin from the laser diode, it repeatedly bounces around in a crystal called the Non-Planar Ring Oscillator consisting of a crystal. It then gets amplified to 200 W in two devices having four laser amplifier rods called the Master Oscillator Power Amplifier and a High Powered Oscillator. Not only are LIGO's mirrors the most reflective in the world, it also has the 2nd largest vacuum in the world, after the Large Hadron Collider. A combination of methods was used for this the first time, including heating the tubes to about 160 degrees Celsius and using Turbo-pump vacuums and ion pumps for 40 days to prevent the light scattering due to dust and air particles. This pressure in the tubes was reduced to one-trillionth that of air pressure at sea level to ensure that we detect true gravitational waves.

LIGO's great sensitivity means that it is also capable of sensing nearby traffic, movement in tectonic plates like earthquakes, and weather changes, among many other disturbances. Using computers, the internal seismic isolation platform (active damping system) nullifies environmental disturbances by generating counter-movements to those vibrations. LIGO's passive damping system uses a quad, a 4-stage pendulum, and hangs the mirrors to it using silica thread twice the thickness of a human hair to keep it motionless. It is also why two

detectors were built quite far apart as gravitational waves, unlike local noises, which would pass through both detectors almost simultaneously.

The sensitivity of LIGO has improved considerably since O1 and O2 [6]. There are a few other gravitational-wave detectors around the world with different detection efficiencies. Germany's GEO600 detector construction is 600 meters long. Virgo (Pisa, Italy) joined LIGO and Germany's GEO600 detector in 2017. Japan's KAGRA detector, the first underground gravitational-wave observatory, became operational on 25 February 2020. There are also many efforts being put into promising future projects! LIGO India project's construction is expected to be completed in the next four to five years. The European Space Agency (ESA) expects to place Laser Interferometer Space Antenna (LISA), a space probe, into solar orbit in about ten years. ESA had launched the LISA pathfinder in 2015 to demonstrate the key technologies and eventually make way for LISA. TianQin is another space-borne gravitational-wave observatory project proposed by the Chinese.

### **Compact Binary Inspiral gravitational waves**

Compact Binary Inspiral gravitational waves are one of the four main types of gravitational waves. They are generated during the final life stages of binary systems, i.e. when the two constituents of the system start to merge. The orbital speed increases and the orbital radius decreases as they spiral closer to each other due to loss in energy in the form of gravitational waves. The frequency and intensity of the gravitational waves increase while the two objects (usually two black holes, two neutron stars, or a black hole and a neutron star) rotate around each other until they merge. [7] We can calculate the spin by evaluating the effect of the black hole's angular momentum that whirls spacetime on the surrounding space and objects.

In the case of a BBH system, we work with the combination of the two black holes' spins through something called the effective inspiral spin parameter (as it is the best-measured spin-related parameter),

$$\chi_{eff} = \frac{m_1 a_1 \cos(\theta_1) + m_2 a_2 \cos(\theta_2)}{m_1 + m_2}$$

where  $m_1$  and  $m_2$  are the masses of the two black holes (primary and secondary respectively),  $\theta$  is the angle between the direction of each BH's spin and the orbital angular

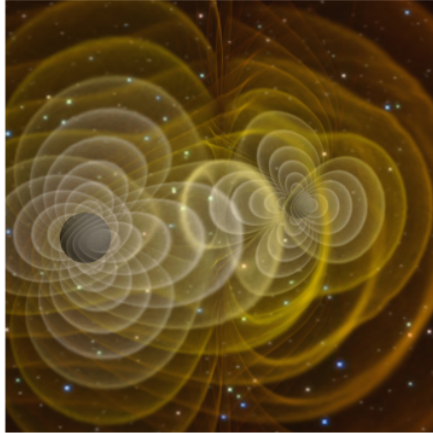


FIG. 4: Gravitational waves produced by two black holes orbiting each other [8]

momentum of the BBH, and  $a_1$  and  $a_2$  each of their dimensionless spin found using

$$a = \frac{cJ}{GM^2}$$

Here,  $c$  is the speed of light,  $G$  is the gravitational constant,  $J$  and  $M$  are the angular momentum and mass of the black hole.

The dimensionless spin magnitude can be between 0 (non-spinning, i.e., a Schwarzschild black hole) and 1. A spin magnitude of 1 or larger would give a naked singularity, and this means that it hit the singularity before crossing the event horizon. This is not possible according to general relativity.

Spin is a vector: it has both magnitude and direction. The direction is given by the right-hand rule. That is, take your right hand and wrap your fingers around in the direction the black hole is spinning. The direction in which your thumb points is the direction of the spin.

We could use either the spherical coordinate or cartesian system to describe the direction the spin is pointing at. However, the Cartesian system is used to generate gravitational waves. The origin is chosen to be at the center of mass of the binary and the  $z$ -axis pointing in the same direction as the orbital angular momentum at some reference time. The  $x$  and  $y$  axes are chosen to point along some arbitrary direction (some models choose the  $x$ -axis to point to the larger object at that time, but this can vary depending on the model). The

projection of the spin vector onto the cartesian coordinate system is  $\text{spin1}x$ ,  $\text{spin1}y$ , and  $\text{spin1}z$  for the primary black hole and  $\text{spin2}x$ ,  $\text{spin2}y$ , and  $\text{spin2}z$  for the secondary black hole.

We should keep in mind that these individual spin components are not very well measured, especially  $\text{spin1}x$ ,  $\text{spin1}y$ ,  $\text{spin2}x$ , and  $\text{spin2}y$ . It is difficult to find the measured values of these parameters very easily. From an astrophysics perspective, the  $x$  and  $y$  components aren't very useful or interesting. The researchers are most interested in the  $z$  component and the total in-plane magnitude (i.e.,  $\sqrt{x^2 + y^2}$ ), since those determine whether or not the binary is precessing. A higher in-plane spin can indicate that the binary formed from dynamical capture rather than two stars in a binary both collapsing to black holes.

The relation between the final spin and  $\text{spin1}x$ ,  $\text{spin1}y$ , and  $\text{spin1}z$  is actually a little complicated. It depends on both the component spins and masses of the binary. We cannot do a simple mapping between the two. Scientists have come up with fitting functions through numerical simulations of binary black hole systems. A PyCBC function makes use of one of them:

```
from pycbc import conversions
final_spin = conversions.final_spin_from_initial(mass1, mass2, spin1x,
spin1y, spin1z, spin2x, spin2y, spin2z)
```

The two black holes get very close before merging if their spins are large and rotate in the same direction as their orbital rotation. They will merge at a greater separation and give a shorter gravitational-wave signal if they spin in the opposite direction to their orbital rotation. If the spins and orbital rotations are not aligned, we see a spin-precession, i.e., the whole binary wobbles as the merger takes place.

Mainly, two different mechanisms have been proposed to understand how a BBH is born and grows: assembled in the field through stellar evolution and a potential common envelope phase, assembled dynamically, either in nuclear star clusters, globular, hierarchical triple, or higher-order stellar systems. Spin mass distributions predicted by them are different. The former case suggests that the black holes' spins are preferentially aligned with the orbital angular momentum, while the latter one indicates that the spin is isotropically distributed with respect to the angular momentum.

There are 15 BBH parameters and 2 more parameters for Binary Neutron Systems. The gravitational-wave signals give us information about the intrinsic and extrinsic properties of the source. Intrinsic properties include mass, spins, tidal deformations, etc., and extrin-

sis properties include distance, inclination, coalescence time, etc. Sources of gravitational waves are pretty simple, and thus it is easy to link our models, i.e., predictions, with the data. Based on the data, we can make predictions using Bayesian inference and parameter estimation.

The image shows the Bayesian inference equation:  $p(\theta|d, M) = \frac{\mathcal{L}(d|\theta, M) \pi(\theta|M)}{\mathcal{Z}(d|M)}$ . Handwritten labels with arrows point to each part: 'Posterior' points to the left side of the equation, 'Likelihood' points to  $\mathcal{L}(d|\theta, M)$ , 'Prior' points to  $\pi(\theta|M)$ , and 'Evidence' points to the denominator  $\mathcal{Z}(d|M)$ .

FIG. 5: Bayesian inference [9]

The image shows the gravitational wave likelihood equation:  $\mathcal{L}(d_i|\theta) = \frac{1}{2\pi P_i} \exp\left(-2\Delta f \frac{|d_i - h_i(\theta)|^2}{P_i}\right)$  and  $\mathcal{L}(d|\theta) = \prod_i^N \mathcal{L}(d_i|\theta)$ . Handwritten labels with arrows point to parts of the equations: 'PSD' points to  $2\pi P_i$ , 'frequency resolution' points to  $\Delta f$ , and another 'frequency resolution' label points to  $P_i$ .

FIG. 6: Gravitational wave likelihood [9]

The above-displayed equations show the Bayesian inference equation. Bayesian inference is a method of statistical inference where Bayes' theorem is used to change the probability for a hypothesis as more information becomes available.

The physical parameters of the candidate event gravitational-wave signals are inferred by computing their posterior probability density functions. The uncertainty in the source parameters is quantified by the posterior probability distribution  $P(\theta|\mathbf{D})$ , which is calculated using Bayes' theorem as,

$$P(\theta|\mathbf{D}) = P(\theta) \frac{P(\mathbf{D}|\theta)}{P(\mathbf{D})}, \quad (1)$$

where  $\theta$  is the set of model parameters,  $\mathbf{D}$  is the data,  $P(\theta|\mathbf{D})$  is the posterior distribution,  $P(\theta)$  is the prior probability distribution for the parameters,  $P(\mathbf{D}|\theta)$  is the likelihood of the data given the model parameters  $P(\theta)$  and  $P(\mathbf{D})$  is the evidence. The likelihood is calculated

from a coherent analysis of data from each detector. In this paper, we assume that the noise can be treated as Gaussian and stationary.

As depicted in FIG. 4, the likelihood is the probability of the detectors measuring data  $D$  assuming signal hypothesis  $M$  and parameters  $\theta$ . Thus, we see from FIG. 5 that the likelihood is dependent on parameters, including the spin.

Phenomenological gravitational waveforms, i.e., approximants, help us computationally predict details about data  $D$  given the parameters  $\theta$ . To detect binaries, we use various waveform models, each with different properties, parameter values, and modeling techniques. These signal models determine the likelihood function. Calculating posterior probability for the fifteen parameters would make us compute  $10^{15}$  likelihood evaluations. All of these simulations require a lot of computational power and time.

The template bank does not have to focus on the extrinsic parameters as much as we have the information about the sky location. Since waveforms are considerably affected by the mass terms, we only generated templates in the 2-D parameter space in O1. However, as the detectors became more sensitive, members of LIGO discovered that template banks designed to cover the Binary Neutron Star systems range lose roughly 6% sensitivity by not accounting for spins [3]. Thus to increase sensitivity, other parameters like a black hole's spin components in the z-direction were taken into account.

Scientists identify candidates using two methods, the first one being to search for minimally-modeled sources. The second method searches for similar signals from a bank of template waveforms [10] which are modeled based on general relativity [11]. The coalescence of binary systems is usually explained in three phases: the inspiral, the merger, and the ring-down. Analytic description of the inspiral phase can be done through the Post-Newtonian expansion. The ring-down is also described by an analytical model [12], as it describes the damped oscillations in the binary coalescence as a superposition of black-hole quasi-normal modes, i.e., modes through which a disturbed object's or field's energy is dissipated. The merger phase is non-perturbative and is described instead by numerical simulations. Numerical relativity simulations are used to generate reference templates. This is done using intrinsic parameters that are determined using the Bayesian parameter estimation studies. Accurate analytic solutions of Einstein's equations are extremely hard to obtain. Thus, we use approximations instead of running programs on supercomputers for days. Data-analysis-ready models are based on families of waveforms like the Taylor, the

effective-one-body, and the Phenom family of waveforms.

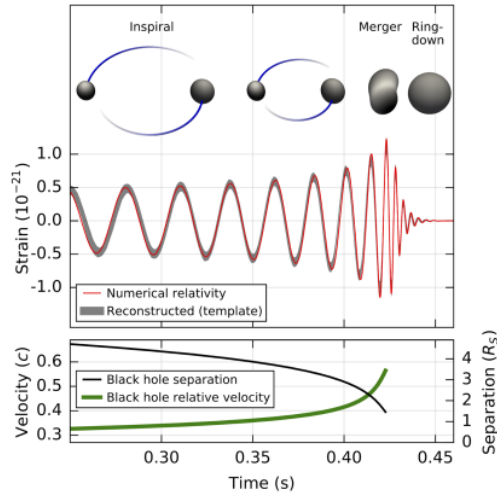


FIG. 7: Reconstructed gravitational-wave strain vs the waveform computed from general relativity. [13]

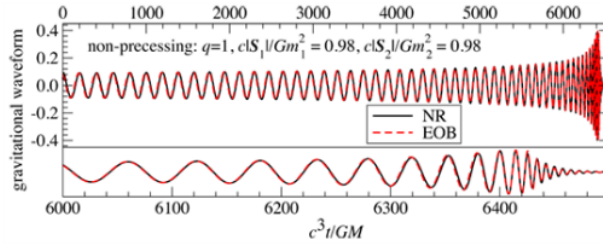


FIG. 8: Two waveforms for the inspiral and merger of two black holes generated using different methods. [13] Image: UMD/AEI.

I chose six events for this project: GW150914, GW151226, GW190814, GW190514\_065416, GW190521, and GW190517\_055101. These six events are quite special and unique.

GW150914 was the first event detected by LIGO on 14 September 2015, at 5:51 a.m. Eastern Daylight Time (09:51 UTC).

GW151226 was the second event detected by LIGO. It was determined that one of the

black holes was spinning at about 20% of the maximum spin rate allowed by general relativity. The final black hole resulting from the merger was spinning at 70% of its maximum possible value. [14]

GW190814's black holes have a huge mass difference: a  $23 M_{\odot}$  black hole and a  $2.6 M_{\odot}$  compact object, making the smaller one either the lightest black hole or heaviest neutron star observed in a binary. However, comparisons with the maximum neutron star (NS) mass predictions using the NS equation of state and electromagnetic observations suggest that the  $2.6 M_{\odot}$  compact object is too heavy to be an NS. Also, GW190814's dimensionless spin magnitude is constrained to lesser than or equal to 0.07. [15]

GW190514\_065416 is a BBH with the smallest effective aligned spin, and GW190517\_055101 is a BBH with the largest effective aligned spin of all O3a events. [16]

GW190521, detected on 2 September 2020, is the heaviest gravitational-wave binary observed ever. The merger resulted in the formation of a black hole of  $142 M_{\odot}$ . This is the first clear detection of an intermediate-mass black hole. [16]

## METHOD

The GW Open Data Workshop No. 4 conducted by LIGO has a series of lectures, tutorials, and quizzes on how LIGO analyzes its data. Its tutorials (on Google Colab) enable us to edit the code. Information about all of the gravitational-wave mergers can be accessed through the `pycbc.catalog` package. I have included all of the code used in this project in a google colab notebook. [17]

PyCBC [18] is an open-source software written in Python and plays a very integral role in data analysis. For instance, it contains algorithms for Fast Fourier Transform, matched filtering, gravitational waveform generation. It has been used since the first direct event detection, i.e., the detection of GW150914 in 2015.

Multiple data conditioning steps are used before analyzing the time-domain data to reduce poor data quality. Here we have assumed that there are no data gaps in our merger signal data. Data gaps are filled with NaNs. "Not a Number" values, in DataFrame and NumPy arrays, represent the absence of a value. After getting the data, we remove the low-frequency content and reduce the sample rate of the data. This is referred to as the preconditioning of data. We notice that there are spikes in the data caused due to this step which is due to the

discontinuity in the data and filter wrap around. We can solve this by trimming the ends of the data. We then want to weigh the frequency components by the noise amplitude by calculating the Power Spectral Density. PSD is the measure of signal's power content versus frequency. It shows at which frequencies energy is strong and at which frequencies energy is weak. Thus, we take the time series equivalent of the multiplicative inverse of PSD and filter the data with it.

The waveform can be generated as a time series using `get_td_waveform()`. In this project, I have decided to use three very different approximants: IMRPhenomXPHM, SpinTaylorT5, and SEOBNRv4\_opt. SEOBNRv4\_opt models the gravitational waveform of inspiraling and merging black holes and includes the ability for each black hole to spin in the same direction as the orbit. Thus, we can only change `spin1z` and `spin2z` parameters. On the other hand, IMRPhenomXPHM, a phenomenological model for gravitational waves from precessing BBH systems, also deals with the dynamics of the in-plane components of the spins. The P in IMRPhenomXPHM stands for precessing. IMRPhenomXPHM is better for the frequency domain, while SEOBNRv4\_opt is better for the time domain. IMRPhenomPv2 and SEOBNRv4PHM are some of the other approximants that also make use of the  $x$  and  $y$  spin components. The waveform section on the PyCBC website gives the list of approximants that are currently available, discusses plotting time-domain waveforms, and calculating the match between waveforms [19]. IMRPhenomXPHM [20] was presented as a model in May 2021. SEOBNRv4\_opt [21] was discussed as the optimized version of SEOBNRv4 in 2016. SpinTaylorT5 [22] is almost 10 years old.

These waveforms models are very different than each other. FIG.[9] shows how SpinTaylorT5, SEOBNRv4\_opt, IMRPhenomPv2, and IMRPhenomXPBM compare when superimposed on one another given fixed parameter values.

We then shift the waveform by the `cyclic_time_shift` method to follow the convention of making sure that the merger is in the first part of the data. Next comes the matched filtering technique, which relies on a model of the signal being dependent on the source physical parameters. To find out the strength of the signal in the data that matches the template in the data, we compute the SNR (signal-to-noise ratio). If the signal aligns with our template, we will get a large value when integrated over. The value of the SNR is proportional to the amplitude of the signal buried in the noise. I applied the PyCBC matched filtering algorithm using the `matched_filter` method. Before calculating the SNR, we re-

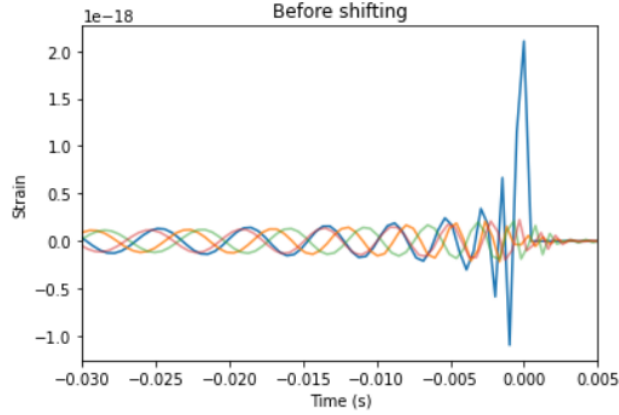


FIG. 9: Here,  $\text{spin}1z=0.199$ ,  $\text{spin}2z=0.999$ . SpinTaylorT5 is colored blue, IMRPhenomPv2 orange, IMRPhenomXPHM green, and SEOBNRv4\_opt red. [3]

move 4 seconds at the beginning and end for the PSD filtering and four more seconds at the beginning to take care of the corruption caused by PSD and template filters. We take the absolute value of SNR as the matched filter function returns a complex SNR. While the real part corresponds to the SNR we get by filtering the template with the data, the imaginary part corresponds to the template 90 degrees out of phase.

#### SNR's change with spin values and the waveform model used

After preconditioning the data, applying a filter to the boundaries, calculating the Power Spectral Density, I varied both the  $\text{spin}1z$  and  $\text{spin}2z$  by 0.1 (whose values range from -1 to 1) and used 3D Plotting in Matplotlib for Python to show their relationship to SNR, after calculating the signal-to-noise time series for our template. Thus, for each of the six events, the two detectors, and three approximants, I have 441 values for each of the three:  $\text{spin}1z$ ,  $\text{spin}2z$ , and SNR. Thus, in total, I generated 36 surface plots and found the peak SNR value and the corresponding  $\text{spin}1z$  and  $\text{spin}2z$  values. I have made a table to summarize my results for each of the events for this paper. I also downloaded the posterior files for these events to verify my values. I have included their values in the table for comparison. I have also included all of the surface plots and the values at .

GWOSC has only released the spin magnitude and polar angle for some events. Thus to

find the individual spin parameters, I downloaded the posterior files for the various events from the Python Software for Gravitational-wave Astronomy's 3-ogc GitHub repository. It has the posterior files for 58 events. Those files are hdf files. I downloaded the files and opened them in Google Colab. PyCBC has pre-written functions to read the hdf file and abstract the data. In them, all three components of the spin vectors are described in spherical coordinates, `spin1_a`, `spin1_azimuthal`, and `spin1_polar`. To convert into cartesian, I used the spherical to cartesian transformations. We can use the fact that  $\text{spin1}_z = \text{spin1}_a \cdot \cos(\text{spin1}_\text{polar})$ . So, for example, to get the components for GW150914, I downloaded its hdf file and imported the required modules. We get numpy arrays having posterior samples of each parameter. I then used `numpy.median("parameter name")` to get the measured value.

I also wanted to get the SNR value from the hdf file. We want a function that returns SNR computed from the given log-likelihood ratio(s). Fortunately we see that we can use `snr=pycbc.conversions.snr_from_loglr(loglr)` to convert loglr to SNR. Thus, we have a parameter space where a particular SNR corresponds to specific values of `spin1x`, `spin1y`, `spin1z`, `spin2x`, `spin2y`, and `spin2z`.

### **Checking for residue after subtracting template from data**

We have found the peak in the SNR value in the previous section. But we want to know if the peak in the signal is the SNR itself. We want to check if our waveform template is efficient, i.e., aligns with the signal precisely. Having found the peak in the SNR value for various events, we can now subtract our proposed template from the data to check the power residue. Since we know where the SNR peak is, we can easily align our proposed signal with the data. We have to concentrate on the important frequency range and compare the data and signal in the same manner. We will whiten both the template and the data, and then bandpass, i.e., letting only the signals between two specific frequencies pass, both the data and template between 30-300 Hz. Whitening the data is dividing it by the noise amplitude spectrum in the Fourier domain. Noise fluctuations are much more significant at low and high frequencies and near spectral lines. Bandpassing gets rid of such noise fluctuations. After following the above steps, we get the data and template in the proper alignment. Since they are now aligned, we subtract one from the other and check if there is a residue in the

time-frequency plot. Having no residue means that our template matches the signal entirely. Having some residue gives us an estimate of how much the template matched the signal.

### **Generating a fake strain**

We use the PSD estimate from one of the events' data so that it doesn't turn out to be too unrealistic. For instance, I got the GW150914 data from the Hanford detector, removed the low-frequency content, downsampled the data to 2048 Hz, and removed 2 seconds of data from both the beginning and end. We then estimate the power spectral density the same way as before.

We continue to reload the strain to use its `delta_t` and `length` to generate our fake strain. We then make a waveform with known spins to compare against. In the project, I generated three strains with different spin parameters. This is our new "strain," so we set the `delta_t` and resize the length to that of the original data strain. Our "strain" is now the plus polarisation of that waveform. The actual strain in the detector would be a linear combination of the polarisations and the detector response function (DRF) for these. We treat it like the original strain and continue with the same steps as before. Remove the low-frequency content and downsample the data to 2048Hz. We again remove 2 seconds of data from both the beginning and end. We make a template with different spins and produce the SNR and resize the vector to match our data. We remove time corrupted by the template filter and the PSD filter.

The SNR we find is quite high, and that is because the template used as the strain is generated with some random amplitude. As the SNR depends on the amplitude, we get a large value here. We should keep in mind that the amplitude arriving at the detector would be much smaller. If we considered the large distance to the source, the amplitude would have been very different. But the absolute value is irrelevant as we want to check the relative influence of changing the spin parameters on the SNR.

## **RESULTS**

The following figures show the relationship between the SNR, `spin1z`, and `spin2z` values and the waveform model used. I have included all of the 36 surface plots, the overlap between

the template and data, visualization of the residue, and the fake strain examples with other events in another document due to the lack of space here [23].

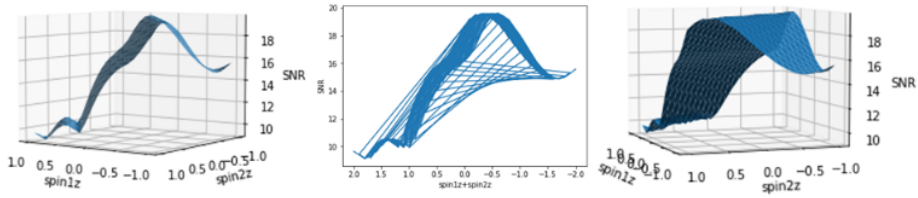


FIG. 10: GW150914's data from LIGO Hanford. IMRPhenomXPHM approximant used. The middle plot shows that the nature of the plot between  $\text{spin1z}+\text{spin2z}$  and SNR is similar to the 3D plot.

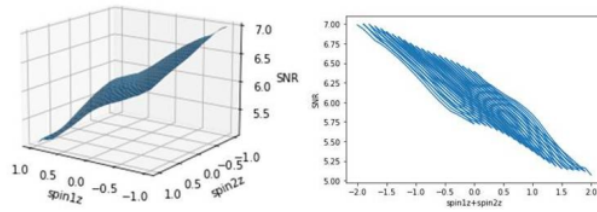


FIG. 11: GW190521's data from LIGO Hanford. IMRPhenomXPHM approximant used. Relative to the other plots, the curve looks flat here.

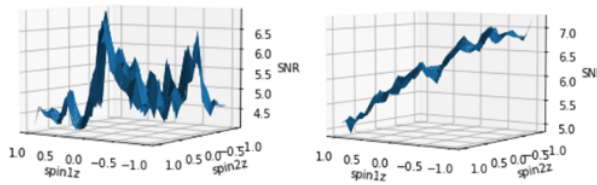


FIG. 12: GW190521's data from LIGO Hanford. SpinTaylorT5 (left) and SEOBNRv4\_opt (right) approximants used respectively. We see a stark contrast between the plots for the same event due to the different approximants used.

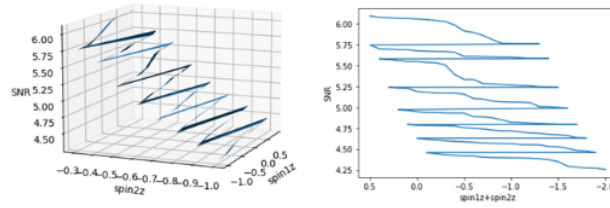


FIG. 13: GW151226's data from LIGO Livingston. SEOBNRv4\_opt approximant used here. This plot looks quite unique in comparison to the other plots I generated as it does not have wavy features or valleys and spikes in the plot.

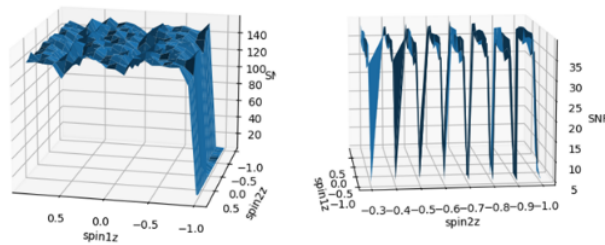


FIG. 14: SEOBNRv4\_opt approximant used. Left: GW190814 from LIGO Hanford. Right: GW151226 from LIGO Hanford. These plots also have unique shapes found in no other plots.

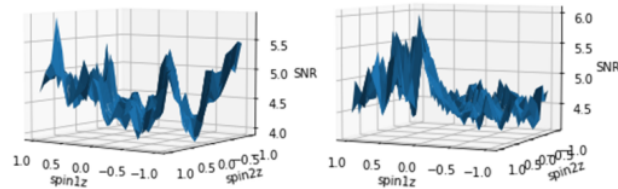


FIG. 15: SpinTaylor T5 approximant used. Left: GW190514.065416 from LIGO Livingston. Right: GW190517.055101 from LIGO Livingston.

We already have the released spin component and SNR values for each of the events from the hdf file. From the plots showing the posterior samples below, we see that except for the graph between  $\text{spin}1z$  and  $\text{spin}2z$ , all of the other graphs have the points taking the shape of a circle. This means that we cannot find out their values as each could be the spin component of the black hole, i.e., their distribution appears to be equal. All of the points in the graph between  $\text{spin}1z$  and  $\text{spin}2z$  populate the region close to the diagonal. The black hole having the higher mass in a BBH has a larger angular momentum than the other. Previously we have seen that the spin is directly proportional to the angular momentum. Since the angular momentum is conserved, as  $\text{spin}1z$  increases,  $\text{spin}2z$  decreases, and vice versa.

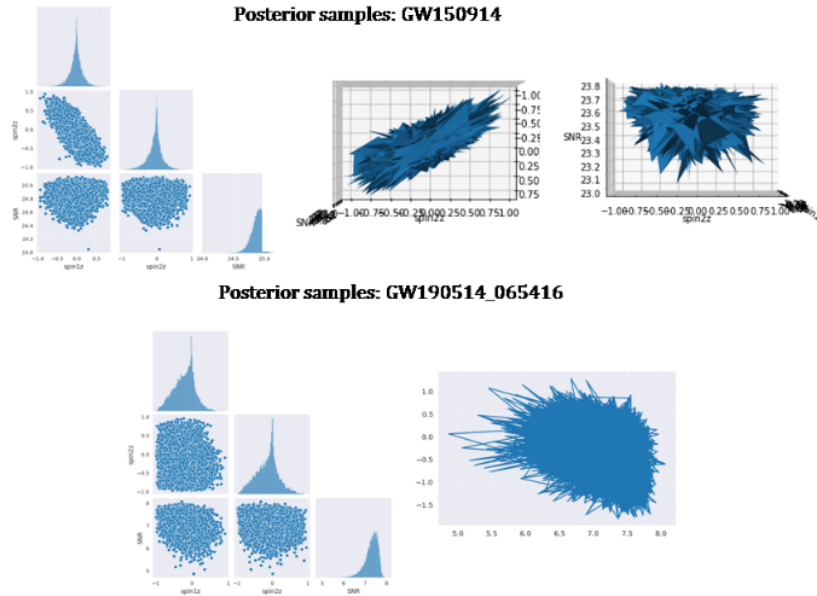


FIG. 16: The plots are from the posterior analysis values. It is interesting to note that while there is a clear diagonal relationship between  $\text{spin}1z$  and  $\text{spin}2z$  in GW150914, it is not quite evident with GW190514\_065416.

### Checking for residue after subtracting template from data

As discussed in the Methods section, checking if there is a residue gives us an estimate of how much the template matched the signal. I plugged in the  $\text{spin}1z$  and  $\text{spin}2z$  values corresponding to the peak SNR value for each of the approximants and events. The color scale in the spectrogram of the data from Hanford in FIG. 17. shows a measure of the power present in the data at a given frequency and time. We can see the "chirp" signal if it's a BBH, as this type of signal is characteristic of compact binary inspirals.

But GW151226, GW190814, and GW190514.065416 have very faint colors. I was not able to accurately identify if there was a residue in the time-frequency plot. Thus, except for those events, I added another column in the tables describing the overlap between the template and the strain and the amount of residue left after subtraction. I have included the tables for GW151226, GW190814, and GW190514.065416 at the end of this paper.

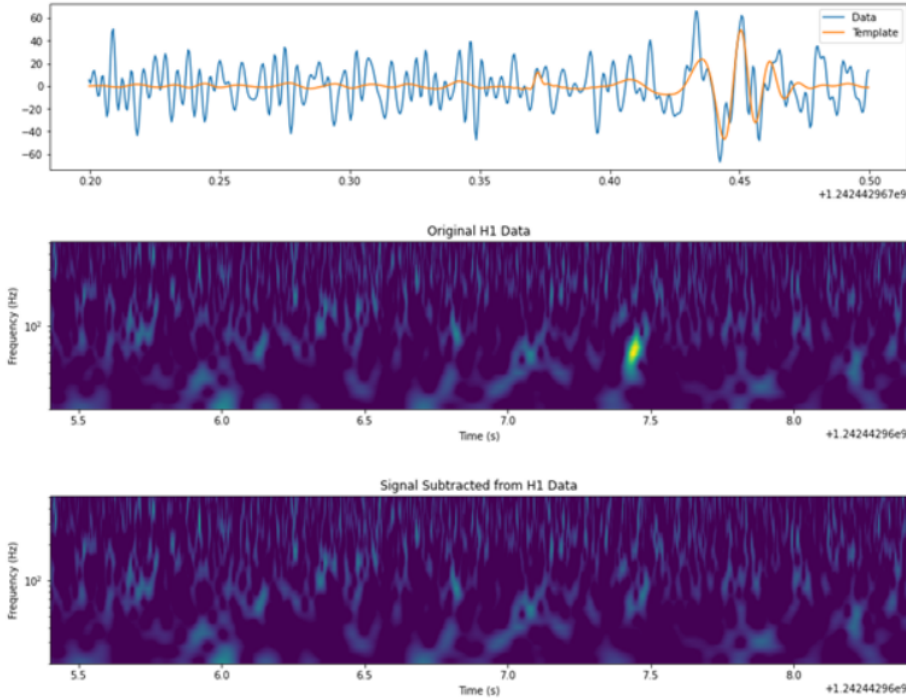


FIG. 17: SEOBNRv4\_opt. There is almost a complete overlap of the template and data and there is no residue left.

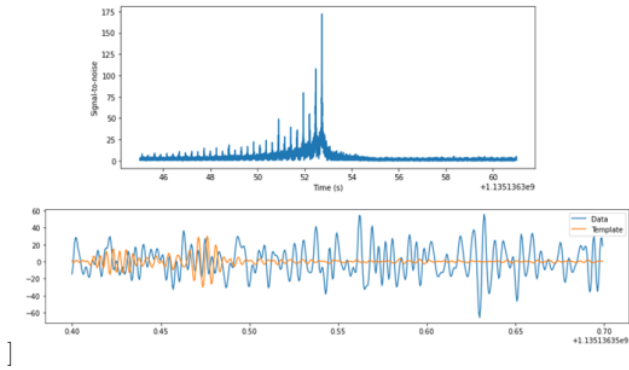


FIG. 18: GW151226 data from LIGO Livingston. The peak SNR value is 171.98. IMRPhenomX-PHM was used here. The template does not overlap much with the strain.

GW150914	Approximant used	Spin1z	Spin2z	Peak in the SNR	Subtracting the Signal from the Data
<b>Hanford</b>	IMRPhenomXPHM	0.3	-0.9	19.62	Perfect overlap. No residue after subtraction.
	SpinTaylorT5	0.3	0.4	15.63	Perfect overlap only at two peaks. Faint residue.
	SEOBNRv4_opt	-0.6	0.1	19.66	Perfect overlap. No residue after subtraction.
<b>Livingston</b>	IMRPhenomXPHM	0.3	-0.7	13.76	Perfect overlap. No residue after subtraction.
	SpinTaylorT5	0.3	0.5	404.99	Almost no overlap. Residue is large.
	SEOBNRv4_opt	-0.5	0.3	26.07	Perfect overlap. No residue after subtraction.
<b>Posterior</b>	IMRPhenomXPHM	-0.008	-0.025	23.82	Perfect overlap. No residue after subtraction.

GW190517_055101	Approximant used	Spin1z	Spin2z	Peak in the SNR	Subtracting the Signal from the Data
<b>Hanford</b>	IMRPhenomXPHM	-0.1	1.0	10.76	Almost perfect overlap. No residue.
	SpinTaylorT5	0.8	-0.6	6.49	Perfect overlap. No residue.
	SEOBNRv4_opt	0.1	0.9	5.96	Partial overlap. Faint residue.
<b>Livingston</b>	IMRPhenomXPHM	-0.8	-0.9	6.68	No overlap at all. There is residue.
	SpinTaylorT5	-0.1	1.0	6.06	Partial overlap. Faint residue.
	SEOBNRv4_opt	-0.5	1.0	6.74	Perfect overlap. No residue.
<b>Posterior</b>	IMRPhenomXPHM	0.709	0.203	11.36	No significant overlap. There is residue.

GW190521	Approximant used	Spin1z	Spin2z	Peak in the SNR	Subtracting the Signal from the Data
<b>Hanford</b>	IMRPhenomXPHM	-1	-0.9	7.00	Perfect overlap. No residue.
	SpinTaylorT5	0.69	-0.30	6.94	Perfect overlap. No residue.
	SEOBNRv4_opt	-1	-1	7.21	Partial overlap. Faint residue.
<b>Livingston</b>	IMRPhenomXPHM	-1	-1	9.66	Partial overlap. Faint residue.
	SpinTaylorT5	-0.50	-0.70	8.42	Partial overlap. Faint residue.
	SEOBNRv4_opt	-1	-1	9.48	Perfect overlap. No residue.
<b>Posterior</b>	IMRPhenomXPHM	-0.416	0.063	15.16	Almost perfect overlap. Faint residue.

We have a mix of results in the last column. While visualizing the overlap between the data and template generated from many of these approximants, we see that some of their peaks don't match. This shows that having a high SNR does not guarantee the accuracy of the corresponding  $\text{spin}1z$  and  $\text{spin}2z$  values. We also see no clear pattern to find out what the  $\text{spin}1z$  and  $\text{spin}2z$  values will be for each waveform model. We have seen from earlier surface plots that the SNR values are almost the same for many of the  $\text{spin}1z$  and  $\text{spin}2z$  values. We also see that the SNR values are abnormally high in some cases. At the same time, some of the  $\text{spin}1z$  and  $\text{spin}2z$  values leave no residue after subtraction.

LIGO has mentioned that they use special-purpose analysis software packages to finalize the parameter values in many of the tutorial pages. They obtain their best-fit templates by selecting a maximum likelihood waveform. The tutorials are not an optimal way of calculating the SNR or finding the residual signal. But they give us an idea of how the SNR changes relative to the change in spin parameters.

Scientists usually do not get a single number for any of the parameters, but instead a probability distribution for it as shown in FIG. 19.

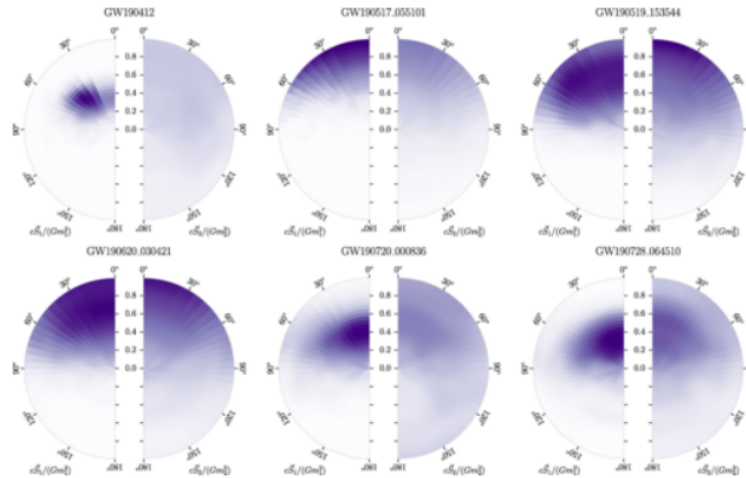


FIG. 19: The colour represents the density of the distribution, where the highest density means the highest probabilities for those parameters. The right semicircle corresponds to the less massive black hole, while the left half corresponds to the heavier black hole. The pixel's radial distance from the circle's center corresponds to the spin magnitude. The pixel's angle from the vertical axis shows the tilt angle between each spin and the Newtonian orbital angular momentum.[11]

Based on the SNR values I got for each detector and waveform model, I calculated the Network SNR. Network SNR is given by [24]

$$(\text{SNR}(\text{Network}))^2 = (\text{SNR}(\text{H1}))^2 + (\text{SNR}(\text{L1}))^2$$

	IMRPhenomX PHM	SpinTaylorT5	SEOBNRv4_opt	Published Network SNR values (PyCBC Search Pipeline)	Posterior samples
<b>GW150914</b>	23.97	405.29	32.65	23.6	23.82
<b>GW151226</b>	172.90	9.89	39.70	13.1	13.24
<b>GW190814</b>	18.52	19.34	158.05	22.2 (GstLAL Search Pipeline)	25.12
<b>GW190514_065416</b>	7.48	8.32	7.68	8.3	8.07
<b>GW190517_055101</b>	12.66	8.88	9.00	10.2	11.36
<b>GW190521</b>	11.93	10.91	11.91	14.2 (IMRPhenomPv3 HM)	15.16

FIG. 20: Network SNR

We see that we get similar Network SNR values mostly for IMRPhenomXPHM. It also looks like SpinTaylorT5's values are a better match than SEOBNRv4\_opt's values.

### Generating a fake strain

We have discussed generating a fake strain in the Methods sections. I wanted to check how the fake strain's surface plots compared to the actual strain's surface plots. How does the absence of noise affect the curve we get in the plot? How is the influence of changing the spin parameters on the SNR different here? I also wanted to check if the change in  $\text{spin1z} + \text{spin2z}$  values had more effects than just the change in the SNR peak values. Thus, I again calculated the change in SNR by varying the spin components for the templates by 0.1 in a nested loop. By following the steps mentioned previously, I get the peak SNR for different values of the spin parameters. Here, I only list three cases where I change the spin values of the fake strain: the posterior samples of GW150914,  $\text{spin1z}=0$  and  $\text{spin2z}=-0.8$ , and  $\text{spin1z}=0.2$  and  $\text{spin2z}=0.3$ . I chose the IMRPhenomXPHM waveform model as it is a very recent model and is perhaps better at generating a strain similar to the actual event's.

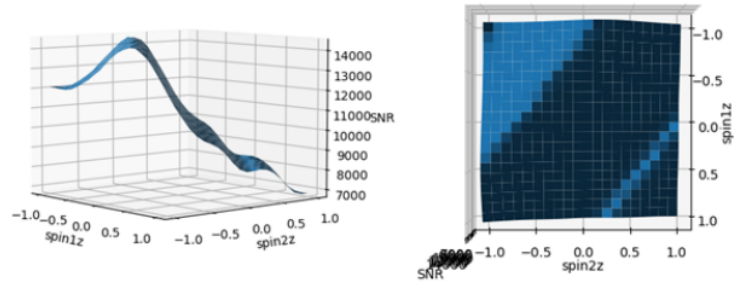


FIG. 21: Approximant IMRPhenomXPHM with  $\text{spin}1z=0$  and  $\text{spin}2z=-0.8$  used as strain. Templates used: IMRPhenomXPHM.

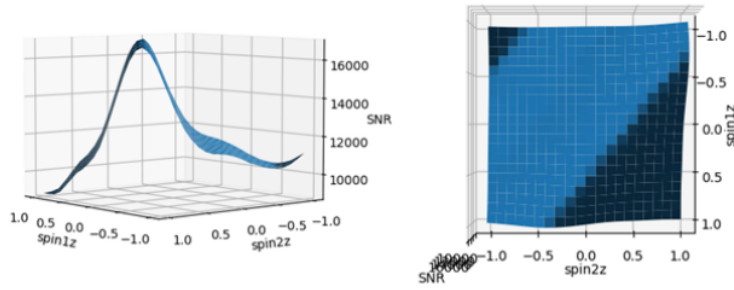


FIG. 22: Approximant IMRPhenomXPHM with  $\text{spin}1z=0.2$  and  $\text{spin}2z=0.3$  used as strain. Templates used: IMRPhenomXPHM. SNR peak shifts here based on the  $\text{spin}1z+\text{spin}2z$  value.

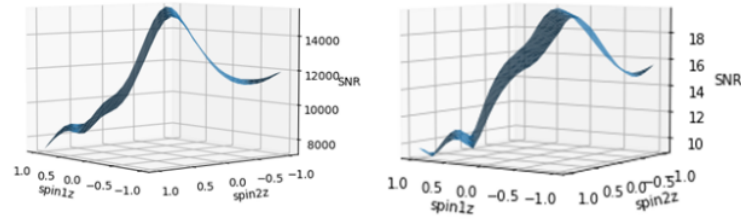


FIG. 23: Left: Approximant IMRPhenomXPHM with  $\text{spin}1x=0.23$ ,  $\text{spin}2x=0.49$ ,  $\text{spin}1y=-0.28$ ,  $\text{spin}2y=0.08$ ,  $\text{spin}1z=-0.22$ , and  $\text{spin}2z=0.16$  used as strain. Templates used: IMRPhenomXPHM. Right: GW150914's data from LIGO Hanford. IMRPhenomXPHM approximant used.

## CONCLUSION

The increasing pace with which gravitational waves are being detected makes us better equipped to understand the nature of black holes. Out of the many parameters, I chose the spin. We observe that there is a relationship between the  $\text{spin1z}$  and  $\text{spin2z}$  values. Instead of a 3D plot, we can capture the same type of information in a 2D plot between SNR and  $\text{spin1z}+\text{spin2z}$ . In the process, we also saw how different approximants, i.e., waveform templates, give different peaks and surface plots for the same parameter values. When the  $\text{spin1z}+\text{spin2z}$  value is changed, keeping the others constant, we find that the peak is shifted. To find the best template match, I subtracted the template from each event's data to check if there is a power residue. For some of the  $\text{spin1z}$  and  $\text{spin2z}$  values, I still got a residue. We also see that IMRPhenomXPBM provides a relatively better match for the Network SNR values.

## SUMMARY

We saw that changing the spin parameters, specifically its z component, also changes the SNR. The SNR changes differently depending on the approximant and event for every small change in the spin values. I also downloaded the posterior samples data files in hdf file format and analyzed them to crosscheck my values. The patterns we observe in the posterior distribution analysis published by PyCBC can also be observed in my data as I change the value of  $\text{spin1z}+\text{spin2z}$ . We also saw that

## FURTHER RESEARCH

The same type of analysis can be done for other events. This would enable us to see more patterns in the relationship between  $\text{spin1z}$ ,  $\text{spin2z}$ , and the SNR values. A more detailed analysis can also compare how a fake strain with no noise would compare to an actual event's strain when filtered with the same template.

## ACKNOWLEDGEMENTS

I would like to sincerely thank Professor Eric Myers at the State University of New York, New Paltz, for his constant guidance, suggestions, and encouragement in choosing a topic and pursuing it for my research project. He introduced me to gravitational waves and patiently helped me with my doubts every step of the way. This project would not have been possible without him.

I also would like to thank Dr. Collin Capano, Postdoctoral Researcher in Gravitational-Wave Astronomy, and Julian Westerweck, a Ph.D. student at the Max Planck Institute for Gravitational Physics, for answering many of my questions relating to the spin parameter and templates.

The availability of extensive collections of data, strain time-streams, parameter estimation samples, and online tutorials enables students like me to familiarize themselves with how LIGO works and help analyze the data. For that, I would like to sincerely thank the LIGO collaboration. In this research project, I have made use of GWOSC, a service by the LIGO Laboratory. The LIGO observatories are built and operated by the LIGO Laboratory (California Institute of Technology and Massachusetts Institute of Technology) with participation by the LIGO Scientific Collaboration and supported by the U.S. National Science Foundation. The Virgo detector is designed, built, and operated by a collaboration between the Centre National de la Recherche Scientifique, the Istituto Nazionale di Fisica Nucleare, and Nikhef, with Polish, Hungarian and Spanish institutes and the European Gravitational Observatory (EGO) consortium.

- 
- [1] Michael Greshko. What are gravitational waves? <https://www.nationalgeographic.com/science/article/gravitational-waves>, 2019. Accessed: 1st July 2021.
  - [2] Interference of waves. <https://www.fizzics.org/interference-of-waves/>. Accessed: 8th July 2021.
  - [3] Ligo's interferometer. <https://www.ligo.caltech.edu/page/ligos-ifo>. Accessed: 8th July 2021.
  - [4] LIGO Scientific Collaboration et al. Advanced LIGO. *Classical and Quantum Gravity*, 32(7):074001, April 2015.

- [5] Stefan L Danilishin, Farid Ya Khalili, and Haixing Miao. Advanced quantum techniques for future gravitational-wave detectors. *Living Reviews in Relativity*, 22(1):1–89, 2019.
- [6] Aaron Buikema, Craig Cahillane, GL Mansell, CD Blair, R Abbott, C Adams, RX Adhikari, A Ananyeva, S Appert, K Arai, et al. Sensitivity and performance of the advanced ligo detectors in the third observing run. *Physical Review D*, 102(6):062003, 2020.
- [7] Sources and types of gravitational waves. <https://www.ligo.caltech.edu/page/gw-sources>. Accessed: 8th July 2021.
- [8] Gms: Simulations uncover 'flashy' secrets of merging black holes. <https://svs.gsfc.nasa.gov/11086>, 2012. Accessed: 23rd July 2021.
- [9] Shanika Galaudage. Parameter estimation with bilby, gw open data workshop. <https://gw-odw.thinkific.com/courses/gw-open-data-workshop-4>, 2021. Accessed: 16th July 2021.
- [10] Benjamin J. Owen and B. S. Sathyaprakash. Matched filtering of gravitational waves from inspiraling compact binaries: Computational cost and template placement. *Phys. Rev. D*, 60:022002, Jun 1999.
- [11] R Abbott, TD Abbott, S Abraham, F Acernese, K Ackley, A Adams, C Adams, RX Adhikari, VB Adya, C Affeldt, et al. Gwtc-2: Compact binary coalescences observed by ligo and virgo during the first half of the third observing run. *Physical Review X*, 11(2):021053, 2021.
- [12] Saul A. Teukolsky. Perturbations of a Rotating Black Hole. I. Fundamental Equations for Gravitational, Electromagnetic, and Neutrino-Field Perturbations. *Astrophys. J.*, 185:635–648, October 1973.
- [13] Ligo scientific collaboration - the science of lsc research. <https://www.ligo.org/science/faq.php>. Accessed: 25th July 2021.
- [14] Gw151226: Observation of gravitational waves from a 22 solar-mass binary black hole coalescence. <https://www.ligo.org/science/Publication-GW151226/index.php>. Accessed: 25th July 2021.
- [15] Richard Abbott, TD Abbott, S Abraham, F Acernese, K Ackley, C Adams, RX Adhikari, VB Adya, C Affeldt, M Agathos, et al. Gw190814: Gravitational waves from the coalescence of a 23 solar mass black hole with a 2.6 solar mass compact object. *The Astrophysical Journal Letters*, 896(2):L44, 2020.
- [16] Gwtc-2: An expanded catalog of gravitational-wave detections. <https://www.ligo.org/>

science/Publication-03aCatalog/flyer.pdf. Accessed: 25th July 2021.

- [17] Shreya Hegde. Google colab notebook for project code. [https://colab.research.google.com/drive/1uiPSVHzFfeXexjS3paqSzJd9twxDEGs\\_?usp=sharing](https://colab.research.google.com/drive/1uiPSVHzFfeXexjS3paqSzJd9twxDEGs_?usp=sharing).
- [18] Alex Nitz et al. gwastro/pycbc: Pycbc release. <https://doi.org/10.5281/zenodo.4849433>, May 2021.
- [19] Waveforms. <https://pycbc.org/pycbc/latest/html/waveform.html>. Accessed: 8th July 2021.
- [20] Geraint Pratten, Cecilio García-Quirós, Marta Colleoni, Antoni Ramos-Buades, Héctor Estellés, Maite Mateu-Lucena, Rafel Jaume, Maria Haney, David Keitel, Jonathan E. Thompson, and Sascha Husa. Computationally efficient models for the dominant and subdominant harmonic modes of precessing binary black holes. *Phys. Rev. D*, 103(10):104056, May 2021.
- [21] Caleb Devine, Zachariah B Etienne, and Sean T McWilliams. Optimizing spinning time-domain gravitational waveforms for advanced ligo data analysis. *Classical and Quantum Gravity*, 33(12):125025, 2016.
- [22] P Ajith. Addressing the spin question in gravitational-wave searches: Waveform templates for inspiralling compact binaries with nonprecessing spins. *Physical Review D*, 84(8):084037, 2011.
- [23] Shreya Hegde. Document for project plots and tables. <https://docs.google.com/document/d/1T1LJWZg4e7kLH6-Nv2UFztrLWBBbLy5TPusUxjtjs08/edit?usp=sharing>.
- [24] Tejaswi Venumadhav, Barak Zackay, Javier Roulet, Liang Dai, and Matias Zaldarriaga. New binary black hole mergers in the second observing run of advanced ligo and advanced virgo. *Phys. Rev. D*, 101:083030, Apr 2020.

<b>GW151226</b>	<b>Approximant used</b>	<b>Spin1z</b>	<b>Spin2z</b>	<b>Peak in the SNR</b>
<b>Hanford</b>	IMRPhenomXPHM	-1.0	-0.1	13.46
	SpinTaylorT5	-0.3	-0.9	7.58
	SEOBNRv4_opt	0.4	-0.4	39.24
<b>Livingston</b>	IMRPhenomXPHM	0.2	1.0	172.38
	SpinTaylorT5	0.2	1.0	6.35
	SEOBNRv4_opt	0.8	-0.3	6.09
<b>Posterior</b>	IMRPhenomXPHM	0.291	0.073	13.24

<b>GW190814</b>	<b>Approximant used</b>	<b>Spin1z</b>	<b>Spin2z</b>	<b>Peak in the SNR</b>
<b>Hanford</b>	IMRPhenomXPHM	-1.0	-0.9	16.28
	SpinTaylorT5	-0.4	0.9	8.85
	SEOBNRv4_opt	-0.2	-0.3	19.00
<b>Livingston</b>	IMRPhenomXPHM	-1.0	-0.1	8.82
	SpinTaylorT5	-0.3	0.6	17.2
	SEOBNRv4_opt	-0.4	0.7	156.91
<b>Posterior</b>	IMRPhenomXPHM	-0.012	0.033	25.12

<b>GW190514_0 65416</b>	<b>Approximant used</b>	<b>Spin1z</b>	<b>Spin2z</b>	<b>Peak in the SNR</b>
<b>Hanford</b>	IMRPhenomXPHM	1.0	-0.1	5.44
	SpinTaylorT5	0.7	1.0	5.85
	SEOBNRv4_opt	0.9	-0.1	5.71
<b>Livingston</b>	IMRPhenomXPHM	0.7	0.9	5.13
	SpinTaylorT5	0.7	0.9	5.92
	SEOBNRv4_opt	1.0	0.3	5.14
<b>Posterior</b>	IMRPhenomXPHM	-0.171	-0.095	8.07